Multiple Configuration Quantum/Classical Studies of the Photodissociation Dynamics of $Ar-H_2O$†

Feng Chen and Anne B. McCoy*

Department of Chemistry, The Ohio State University, Columbus, Ohio 43210

Received: February 28, 2004; In Final Form: July 20, 2004

The results of a multiple-configuration mixed quantum/classical study of the photodissociation dynamics of H_2O ($\tilde{X} \rightarrow \tilde{A}$) and $Ar-H_2O$ ($\tilde{X} \rightarrow \tilde{A}$) are presented. In this approach, the dynamics of the argon atom and one of the hydrogen atoms are treated classically, while the dynamics of the remaining OH molecule is treated quantum mechanically. The quantum subsystem is further divided into two coupled contributions, and separate classical trajectories are propagated for each piece. Comparisons of the rotational distribution of the OH product, obtained from photodissociation of $Ar-H_2O$ and H_2O, are in good agreement with previous classical and experimental studies of these systems. The differences between the properties associated with the photodissociation of water and the argon−water complex demonstrate the influence of the argon atom on the dynamics.

I. Introduction

Understanding how weak intermolecular interactions affect chemical reaction dynamics is an issue of central interest in chemistry. Weakly bound, van der Waals or hydrogen-bonded complexes provide excellent testing grounds for such investigations. They are of particular interest because their small size allows for detailed experimental studies and accurate treatments of potential surfaces as well as detailed theoretical treatments of the dynamics. As a result there have been a number of studies of either photoinduced or bimolecular processes in weakly bound complexes.[1−11]

The challenges in studying reaction dynamics in clusters come from the fact that they often contain more than three or four atoms and the fact that the system will dissociate into three or more fragments. This makes full-dimensional quantum mechanical approaches prohibitively expensive. An alternative approach is provided by classical treatments. Compared to quantum approaches, for which the size of the basis increases exponentially with the number of atoms, the time and memory requirements of classical approaches scale roughly linearly with the number of atoms.

Often, when we consider the dynamics of a reaction in a cluster, most of the dynamics are fundamentally classical, and only a few atoms exhibit significant quantum behaviors. When this is the case, a natural choice is to employ a mixed quantum/classical treatment in which several degrees of freedom are treated quantum mechanically, while the remaining coordinates and momenta are propagated classically. The literature on mixed quantum/classical studies is abundant,[12−15] and much of the work in this field can be traced to the pioneering work of Billing.[16−19]

While mixed quantum/classical approaches have proven to provide powerful tools for studying the dynamics of moderate sized systems, when multiple channels are energetically accessible, as is often the case in reaction or photodissociation dymamics, the quantum wave packet becomes delocalized, and problems arise due to overcorrelations between the quantum and classical dynamics.[7,20] Similar problems have been noted when the dynamics are treated by a separable quantum mechanical wave function. In this case, a multiple configuration time-dependent Hartree approach was developed to solve these problems.[21,22] Building from that work, we recently developed a multiple-configuration quantum/classical approach, and we have applied it to studies of the photodissocation of water and reactions of oxygen with HCl and $Ar-HCl$.[23−26] In this approach, the quantum subsystem is divided into two or more orthogonal wave functions, and classical trajectories are propagated for each of the contributions to the quantum wave packet. This approach provides a more accurate description of the dynamics than the simple Ehrenfest-based quantum classical treatments without introducing significant additional computational demands compared to the single-configuration approach.

In this paper, we use the multiple-configuration mixed quantum/classical approach to investigate how the introduction of an argon atom affects the absorption spectrum and the rotation distributions of the OH products following the photodissociation of water. There are several reasons that we choose to study this system. Recently Nesbitt and co-workers reported the results of experimental studies of vibrationally mediated photodissociation of H_2O and $Ar-H_2O$ van der Waals complexes.[27,28] In these studies, the free OH bond in water (the one that is further away from the argon atom) is selectively dissociated. The resulting OH rotational distributions were recorded and compared with the ones that resulted from the photodissociation of H_2O at the same photolysis wavelengths. Warmer OH rotational distributions were obtained from the photodissocation of water in a $Ar-H_2O$ cluster, compared with OH rotational distributions resulting from the photodissocation of an isolated water molecule. The differences in the OH distributions were explained in terms of an intermolecular collision in the exit channel that transfers energy between the argon atom, the hydrogen atom, and the OH molecule.

The photodissociation of H_2O has been studied extensively by a variety of computational approaches, including time-dependent quantum calculations[29−31] and classical trajectory simulations.[32,33] Partridge et al. developed a high quality ab initio surface[34] to describe the $\tilde{X}$ state of water, and Engel and coworkers developed a potential for the $\tilde{A}$ state.[29] The potential

† Part of the "Gert D. Billing Memorial Issue".

* Corresponding author e-mail: mccoy@chemistry.ohio-state.edu.

10.1021/jp0490958 CCC: $27.50
Published on Web 08/11/2004

energy surface of $\tilde{A}$ state is purely repulsive, and the dissociation dynamics are direct.

In addition, from experimental spectroscopic studies, much is known, about the ground state of the Ar−H_2O van der Waals complex, and, based on this work, an empirical potential was developed by Cohen and Saykally.[35] A potential for Ar−H_2O ($\tilde{A}$) has also been developed. It is based on the previously reported H_2O ($\tilde{A}$) state potential[29] and pairwise interaction between the argon atom and the dissociating H and OH units.[4] These potential energy surfaces were used by Christoffel and Bowman for quasiclassical trajectory simulations for the photodissociation of Ar−H_2O and H_2O with three or four quanta of excitation in the free OH bond in water.[4,5] Consistent with the experiments, these studies indicated a slight increase in the angular momentum of the OH product when the process was initiated in the argon−water complex. They explained this finding in terms of the influence of the Ar−OH interaction, which favors a linear Ar−H−O orientation and induces a torque on the OH bond.

A known difficulty with purely classical approaches is the leakage of zero-point energy out of the higher frequencies OH stretch as well as the removal of the constraints of the angular momentum of the OH product. In the present paper, we describe the results of a mixed quantum/classical treatment of this process in which the OH bond that remains intact is treated quantum mechanically, while the dynamics of the dissociating hydrogen and argon atoms are treated classically.

The remainder of the paper is organized as follows. In the following section, we present the Hamiltonians used in this study and review the quantum/classical approaches taken here. In section III, the results for a planar approximation to the dynamics of the H_2O photodissociation are presented and compared to those obtained for $J = 0$. This is done because the computational challenges of this system make full three-dimensional studies of the Ar−H_2O dissociation computationally prohibitive, and we have elected, as a first step, to consider the dynamics in a plane. The results are compared to those obtained from experiment and previous classical studies.

II. Theoretical Approaches

A. Coordinates and Hamiltonian. In this study of the photodissociation dynamics of argon−water, the complex is confined to a plane. As such, the Hamiltonian is expressed in terms of the X and Y Cartesian coordinates of each of the four atoms. We treat the dynamics of the OH bond that remains intact, quantum mechanically, and the relative motions of the remaining hydrogen, OH, and argon atom, classically. To facilitate this separation, the internal coordinate Hamiltonian is written in terms of the six coordinates ($r,\theta,X,Y,X_{Ar},Y_{Ar}$) shown in Figure 1. Here r and θ provide the length and orientation of the OH bond, while (X_{Ar},Y_{Ar}) are the Cartesian coordinates of the argon atom and (X,Y) provide the Cartesian coordinates of the hydrogen atom. The positions of the hydrogen and argon atoms are referenced to the center of mass of OH. As such, the Hamiltonian is given by

$$\hat{H} = -\frac{\hbar^2}{2\mu_{OH}}\left(\frac{\partial^2}{\partial r^2} + \frac{1}{4r^2} + \frac{1}{r^2}\frac{\partial^2}{\partial \theta^2}\right) + \frac{P_X^2 + P_Y^2}{2\mu_{H-OH}} + \frac{P_{X_{Ar}}^2 + P_{Y_{Ar}}^2}{2\mu_{Ar-OH}} + \frac{P_X P_{X_{Ar}} + P_Y P_{Y_{Ar}}}{m_H + m_O} + V(X,Y,X_{Ar},Y_{Ar},r,\theta) \quad (1)$$

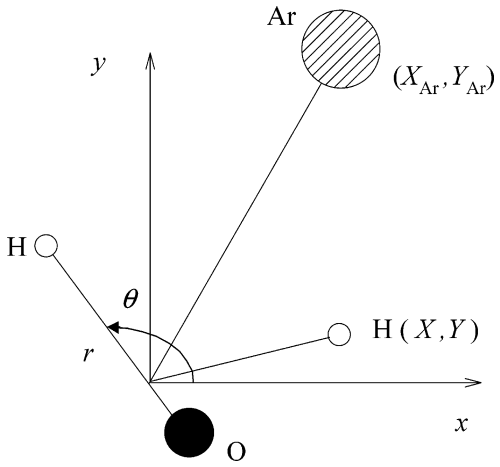

Figure 1. The planar coordinate system used in this study.

where μ_{OH}, μ_{H-OH}, and μ_{Ar-OH} represent the reduced masses of OH, H−OH, and Ar−OH, respectively. The global potential is given by $V(r,\theta,X,Y,X_{Ar},Y_{Ar})$. As in our previous study on the photodissociation of water,[7,26] we use the high quality ab initio surface of Partridge et al.[34] and the potential of Engel and co-workers[29] to describe the $\tilde{X}$ state and $\tilde{A}$ states of water, respectively. The Ar−H_2O intermolecular potential for the $\tilde{X}$ state is given by the sum of H_2O intramolecular potential and the empirical Ar−H_2O potential of Cohen and Saykally.[35] For the $\tilde{A}$ state we use the additive surface that was developed by Christoffel and Bowman for their classical studies on this system.[4] More recently, Jungwirth and co-workers developed an $\tilde{A}$ state surface for Ar−H_2O that is given by an analytical fit to the results of ab initio calculations at the CASPT2 level of theory.[36] In studies on this surface, these workers found that in the regions of the potential that are relevant for photodissociation of Ar−H_2O,[37] the potential of Christoffel and Bowman worked well, and we elect to use that potential in the present studies.

Performing simulations in reduced dimensionality carries with it the danger that the results cannot be extrapolated to the system in its full dimensionality. Such a problem is known to exist for planar treatments of triatomic systems as, although three points form a plane and zero-total angular momentum puts constraints on the conjugate momenta, $J = 0$ is not the same as a planar representation of the dynamics. Rather, $J = 0$ corresponds to an isotropic distribution of orientations. This difference is borne out of the fact that the angular momentum associated with planar motion is proportional to j^2, whereas in three Cartesian dimensions it becomes proportional to $j(j + 1)$.

To test the reliability of the planar representation of the Ar−H_2O photodissociation dynamics, we investigate the photodissociation dynamics of an isolated water molecule in both the planar and three-dimensional ($J = 0$) representations. For the later calculations, we use Jacobi coordinates, r, R, and γ, where r is defined as before, R is the magnitude of the vector between the hydrogen atom and the center of mass of OH, and γ is the angle between r and R. As such, the Hamiltonian in Jacobi coordinates is given by

$$\hat{H} = -\frac{\hbar^2}{2\mu_{H-OH}}\frac{\partial^2}{\partial R^2} - \frac{\hbar^2}{2\mu_{OH}}\frac{\partial^2}{\partial r^2} + \left(\frac{1}{2\mu_{H-OH}R^2} + \frac{1}{2\mu_{OH}r^2}\right)\hat{j}^2 + V(R,r,\gamma) \quad (2)$$

The volume element for integration is $\sin\gamma dr dR d\gamma$. Likewise, the Hamiltonian for water in the planar coordinate representation is given by

$$\hat{H} = -\frac{\hbar^2}{2\mu_{OH}}\left(\frac{\partial^2}{\partial r^2} + \frac{1}{4r^2} + \frac{1}{r^2}\frac{\partial^2}{\partial\theta^2}\right) - \frac{\hbar^2}{2\mu_{H-OH}}\left(\frac{\partial^2}{\partial R^2} + \frac{1}{4R^2} + \frac{1}{R^2}\frac{\partial^2}{\partial\theta^2}\right) + V(R,r,\theta) \quad (3)$$

where θ is the angle between r and R and the remaining coordinates are the same as in eq 2. Here the volume element for integration is $dr dR d\theta$. At first glance, one might expect that θ and γ represent the same coordinate. The difference comes in the range over which they are defined. In the planar coordinate representation $0 < \theta < 2\pi$, while in the Jacobi coordinate representation $0 < \gamma < \pi$.

B. Quantum Simulations. To calibrate the accuracy of the planar approximation, we perform quantum simulations of the photodissociation dynamics of H_2O using the Hamiltonians in eqs 2 and 3. This is achieved by solving

$$\Phi(t) = e^{-i\hat{H}t/\hbar}\Phi(t=0) \quad (4)$$

using a grid representation of the wave function. Likewise, following our previous work, a grid-based approach is also used to evaluate the wave functions on the $\tilde{X}$ state of H_2O.[26] For the Jacobi coordinate representation, the wave functions in the two radial coordinates, r and R, are represented by an evenly spaced grid of points, while a DVR that is based on the Legendre polynomials is used to describe the bending dependence of the wave function. For the calculations in planar coordinates the wave function in all three coordinates is represented on an evenly spaced grid of points. Once the wave functions are obtained, time-dependent quantum approaches are used to propagate the dynamics on the $\tilde{A}$ state potential. In this work we use a Chebychev expansion of the propagator in eq 4.[38,39] Details of this approach are provided elsewhere.[26,40]

C. Mixed Quantum/Classical Treatments. While purely quantum mechanical treatments can be readily applied to studies of the photodissociation of water, the introduction of even a single argon atom makes such simulations prohibitively expensive. Even by introducing the simplification of confining the motions to a plane, such a simulation requires the inclusion of five internal degrees of freedom. Given that the system will dissociate into three units, H + OH + Ar, the size of the grids that would be required to represent the wave function would be prohibitively large. Further, the large recoil energy of H + OH and the large mass of argon mean that the grids in X, Y, X_{Ar}, and Y_{Ar} would need to be very dense. As such, we elect to employ a quantum/classical approach, in which the Ar−H_2O system is divided into two subsystems, one of which is treated quantum mechanically and another that is treated classically. For the photodissociation of Ar−H_2O, the coordinates and momenta of one of the hydrogen atoms and the argon atom, X, Y, X_{Ar}, Y_{Ar}, P_X, P_Y, $P_{X_{Ar}}$, and $P_{Y_{Ar}}$, are treated classically, while the dynamics of the remaining OH molecule, which is described by r, θ, and their conjugate momenta, are treated quantum mechanically.

Employing such a separation of the dynamics in a study of the photodissociation of water requires a set of initial conditions of the form of initial coordinates and momenta for the classical degrees of freedom and a fully coupled wave function for the quantum degrees of freedom. Since the motions of the two OH stretches are coupled even in the ground state of water, we simplify the generation of the initial conditions by reexpressing the wave function for the ground state of Ar−H_2O as a product of two functions, one that depends only on r and θ and one that depends only on the classical coordinates. This is achieved through a natural modal analysis[41] and is described in greater detail in ref 26.

While the motions of one of the hydrogen atoms can be treated classically, the initial conditions for these trajectories must reflect the initial quantum state of the system if we are to have a meaningful description of the photodissociation dynamics. We obtain the initial condition by mapping the R dependence of the initial wave function, $\psi(R)$, onto a phase space distribution using the Wigner function[42,43]

$$W(R,P) = \frac{1}{2\pi\hbar}\int_{-\infty}^{+\infty} ds\,\psi^*\left(R + \frac{s}{2}\right)\psi\left(R - \frac{s}{2}\right)e^{isP/\hbar} \quad (5)$$

where $W(R,P)$ provides the weight of each trajectory. In this work, the initial conditions for R and P are based on an evenly spaced grid of points with R ranging from 1.44 to 2.37 a_0 and P ranging from −13.6 to +13.6 au. This grid is divided into 6400 equal sized rectangles by dividing the R and P ranges into 80 equal units. The initial conditions are selected randomly within each of these boxes. We choose to take this approach rather than using the grid points themselves since there is a strong correlation between the initial value of P and the final kinetic energies of the argon and hydrogen atoms. Finally, only those trajectories whose magnitude of the $W(R,P)$ exceeds 10^{-3} are propagated.

As eq 5 implies, the ground-state wave function for this hydrogen atom depends only on the magnitude of **R**, rather than its Cartesian components. As such, at $t = 0$, this hydrogen atom is on the positive x-axis and the y component of its momentum is zero. Likewise, the argon atom is initially placed at its equilibrium configuration, obtained from the ground-state potential. The initial momentum of the argon atom is also zero. We tested the sensitivity of the results to the position of the argon atom and found that while the total and partial cross sections display a small sensitivity to the direction of R_{Ar}, they are relatively insensitive to the magnitude of this vector within the range sampled by the ground-state wave function.

Finally, it should be noted that there are two possible equilibrium positions for the argon atom. In one the argon atom is near the hydrogen atom that is being treated classically, while the other places the argon atom near the hydrogen atom that is treated quantum mechanically. Because we have broken the symmetry in our treatment of the dynamics, the results for these two cases will no longer be identical and the total cross section is the sum of the cross sections for these two channels.

Once the initial coordinates, momenta, and weights have been determined, we need to develop the equations of motion for the quantum wave packet and the classical degrees of freedom. As we have shown previously, since there are two equivalent channels along which water can dissociate, the simplest quantum/classical treatment, in which a single classical trajectory is propagated along with the quantum wave packet, will provide a poor description of the dynamics.[7,26] As such, we will use the multiple-configuration quantum/classical approach to correct the deficiencies in the quantum/classical approach.[24,26]

In the multiple-configuration quantum/classical approach, we project the quantum wave packet onto two or more contributions, and classical trajectories are propagated independently for each of these contributions. Following the multiple-configuration quantum approach, proposed by Hammerich et al.,[44] we

define a two-configuration treatment through a set of orthogonal projection operators

$$P_1 = \sum_{i=0}^{4} |\phi_i\rangle\langle\phi_i|$$

$$P_2 = \sum_{i=5}^{\infty} |\phi_i\rangle\langle\phi_i| \tag{6}$$

where $|\phi_i\rangle$ represents a vibrational eigenfunction of an isolated OH molecule, obtained by numerically finding the eigenfunctions of the water excited-state potential at large H−OH distances. As such, one of the operators projects out those configurations with four or fewer quanta in the OH stretch. This will correspond to the channel in which the hydrogen atom that is treated classically is the one that is dissociated, while the OH bond that is treated quantum mechanically remains intact. By contrast, P_2 projects out the part of the wave packet in which the quantum mechanical OH bond is broken. As this channel is not treated well by the quantum/classical approximation it will not be considered in our calculation of the cross section. The projection operators satisfy

$$\sum_{n=1}^{2} P_n = 1 \tag{7}$$

and

$$\chi_n(r,\theta,t) = P_n\chi(r,\theta,t) \tag{8}$$

where $\chi_n(r,\theta,t)$ represents the part of the wave packet that is localized in the nth channel. The equations of motion for the two-configuration treatment are

$$-i\hbar\frac{\partial\chi(r,\theta,t)}{\partial t} = \left\{-\frac{\hbar^2}{2\mu_{OH}}\left(\frac{\partial^2}{\partial r^2} + \frac{1}{4r^2} + \frac{1}{r^2}\frac{\partial^2}{\partial\theta^2}\right) + V(X(t),Y(t),X_{Ar}(t),Y_{Ar}(t),r,\theta)\right\}\chi(r,\theta,t)$$

$$\frac{dX(t)}{dt} = \frac{P_X(t)}{\mu_{H-OH}} + \frac{P_{X_{Ar}}(t)}{m_H + m_O}$$

$$\frac{dY(t)}{dt} = \frac{P_Y(t)}{\mu_{H-OH}} + \frac{P_{Y_{Ar}}(t)}{m_H + m_O}$$

$$\frac{dX_{Ar}(t)}{dt} = \frac{P_{X_{Ar}}(t)}{\mu_{Ar-OH}} + \frac{P_X(t)}{m_H + m_O}$$

$$\frac{dY_{Ar}(t)}{dt} = \frac{P_{Y_{Ar}}(t)}{\mu_{Ar-OH}} + \frac{P_Y(t)}{m_H + m_O}$$

$$\frac{dP_\alpha^{(n)}}{dt} = -\frac{\left\langle\chi_n(r,\theta,t)\left|\frac{V(X(t),Y(t),X_{Ar}(t),Y_{Ar}(t),r,\theta)}{\partial X_\alpha}\right|\chi_n(r,\theta,t)\right\rangle}{\langle\chi_n(r,\theta,t)|\chi_n(r,\theta,t)\rangle} \tag{9}$$

where α in the last line of eq 9 represents one of the four Cartesian coordinates or momenta and n can be 1 or 2.

D. Calculating Cross Sections. For the simulations of the photodissociation of water, the asymptotic rotation vibration product state distributions for OH in the planar coordinate representation are calculated from the results of the quantum simulation using[45,46]

$$\sigma_{vm}(\omega) \propto \omega\left(\frac{\mu_{H-OH}}{2\pi\hbar k_{vm}}\right)\lim_{t\to\infty}\left|\int_0^\infty dR\int_{r_{min}}^{r_{max}} dr\int_0^{2\pi} d\theta e^{-ik_{vm}R}\times \phi_{vm}(r)\varphi_m(\theta)\Phi(R,r,\theta,t)\right|^2 \tag{10}$$

where $\varphi_m(\theta)$ represents one of the angular momentum eigenstates of the OH and $\phi_{vm}(r)$ represents the vth vibrational wave function for OH for a given level of rotational excitation. The translational motion of H + OH is described by a plane wave with wave vector, $k_{vm} = [2\mu_{H-OH}(\hbar\omega + E_0 - \epsilon_{vm})]^{1/2}/\hbar$. Here, ω is the photon frequency and E_0 is the initial energy of the water molecule on the $\tilde{X}$ state. ϵ_{vm} is the energy associated with the state ϕ_{vm}. The only differences between the above expressions and those for the cross sections for the Jacobi coordinate representation are that the subscript m should be replaced by j, θ is replaced by γ, and the limits of integration over the angle are from 0 to π, rather than 0 to 2π. Finally angular momentum eigenstates $\varphi_j(\gamma)$ of the OH are Legendre polynomials.

In the quantum/classical simulations, we only consider the planar coordinate representation. Here, the partial cross sections for H_2O are obtained using

$$\sigma_{vm}^{Q/C}(\omega) \propto \omega\lim_{t\to\infty}\left\{\sum_{i=1}^{ntraj}\left(\frac{\mu_{H-OH}}{\bar{k}^{(i)}}\right)W(R^{(i)}(0),P^{(i)}(0))\times \delta(P^{(i)}(t) - \hbar\bar{k}^{(i)})\left|c_{vm}^{(i)}(t)\right|^2\right\} \tag{11}$$

where $c_{vm}^{(i)}(t) = \int_{r_{min}}^{r_{max}} dr\int_0^{2\pi} d\theta\phi_{vm}(r)\varphi_m(\theta)\chi^{(i)}(r,\theta,t)$ and the (i) superscript is used to represent a single trajectory. We use $\bar{\epsilon}^{(i)} = \sum_{vm}c_{vm}^{(i)}\epsilon_{vm}$, to represent the average energy of the quantum wave packet. As such, for a given photon energy, $\hbar\omega$, the wave vector that corresponds to the energy available to the momentum of the dissociating hydrogen atom is given by $\bar{k}^{(i)} = [2\mu_{H-OH}(\hbar\omega + E_0 - \bar{\epsilon}^{(i)})]^{1/2}/\hbar$.

The partial cross section for the two-configuration quantum/classical description of the photodissociation of Ar−H_2O is given by

$$\sigma_{vm}^{Q/C}(\omega) \propto \omega\sum_{i=1}^{ntraj} W(R^{(i)}(0),P^{(i)}(0))\left(\frac{\mu_{H-OH}}{\bar{k}^{(i)}}\right)\times \delta(P^{(i)}(t) - \hbar\bar{k}^{(i)})|c_{vm}^{(i)}|^2 \tag{12}$$

where

$$\bar{k}^{(i)} = \frac{\left[2\mu_R\left(\hbar\omega + E_0^{Ar-H_2O} - \frac{[P_{Ar}^{(i)}(t)]^2}{2\mu_{Ar-H_2O}} - \bar{\epsilon}^{(i)}\right)\right]^{1/2}}{\hbar}$$

is the wave vector that corresponds to the energy available to the classical momentum of the hydrogen atom

$$P_{Ar}^{(i)}(t) = \sqrt{[P_{X_{Ar}}^{(i)}(t)]^2 + [P_{Y_{Ar}}^{(i)}(t)]^2}$$

and

$$P^{(i)}(t) = \sqrt{\left[P_X^{(i)}(t) + \frac{m_H}{m_{H_2O}}P_{X_{Ar}}^{(i)}(t)\right]^2 + \left[P_Y^{(i)}(t) + \frac{m_H}{m_{H_2O}}P_{Y_{Ar}}^{(i)}(t)\right]^2}$$

Here $E_0^{Ar-H_2O}$ is the initial energy of the argon−water complex on the $\tilde{X}$ state. This final transformation is necessary in order to remove the cross terms from the calculation of the total kinetic energy.

To evaluate the δ-function in eqs 11 and 12, we follow Henriksen, Engel, and Schinke[32] and use

$$\delta(z) = \frac{1}{\sqrt{\gamma^2\pi}} e^{-(z/\gamma)^2} \tag{13}$$

In this work, $\gamma = 4 \times 10^{-3}$ H.

Another quantity of interest is the probability that a kinetic energy (E) has been transferred to the Ar atom. This is obtained using

$$P(E) = \sum_{i=1}^{ntraj} W(X^{(i)},Y^{(i)},P_X^{(i)},P_Y^{(i)})\, \delta\left\{\frac{[P_{Ar}^{(i)}(t)]^2}{2m_{Ar}} - E\right\} \tag{14}$$

where the δ-function is replaced by eq 13 with $\gamma = 2 \times 10^{-4}$ H.

E. Numerical Details. In the quantum wave packet propagations, we use grids in R and r ranging from 0.5 to 15.5 a_0 with 128 grid points in each dimension. 64 grid points are used in θ, while 30 grid points are used in γ. Since the system can dissociate along either R or r, absorbing potentials are introduced in each coordinate, where[47]

$$f(x) = \begin{Bmatrix} 0, & x_I < x \\ 10y^3 - 15y^4 + 6y,^5 & x_I \le x \le x_I + \Delta x \\ 1, & x_I + \Delta x < x \end{Bmatrix} \tag{15}$$

where

$$y = \frac{x - x_I}{\Delta x} \tag{16}$$

The parameter x_I provides the value of r or R where the absorbing potential becomes nonzero and Δx provides the range of the absorbing potential. In this study, we use $R_I = r_I = 11$ a_0, and $\Delta R = \Delta r = 3$ a_0. We propagate the wave packet for 3000 au with a time step of 200 au. This is the time that is required for most of the wave packet to reach the asymptotic region of the potential. When part of the wave packet reaches the asymptotic region of the potential, it is projected onto the asymptotic states that are used to evaluate the cross section in eq 10. Further propagations of this part of the wave packet are carried out analytically.[45]

In the two-configuration quantum/classical studies, we use a 64-point grid in r that ranges from 0.5 to 8.5 a_0 and 128 grid-points in θ. The absorbing potential that is used for r has the same form as we use for the three-dimensional quantum simulations. It should be noted that the absorbing potential will only affect the dynamics in channel 2, the part of the wave packet that we do not consider in evaluating the forces on the classical particles. We use a 0.2 au time-step for solving both the classical and quantum equations of motion when $R < 4$ a_0. For larger values of R a 1.0 au time step is used. Given the short time steps, a split operator propagator is used to propagate the quantum dynamics, and a simple second-order differencing scheme is used to solve the classical equations of motion.[40,48]

The cross sections that are reported for the two-configuration quantum/classical simulations are based on 6400 trajectories. It should be noted that because the angle between the two OH bonds is defined in the range from 0 to 2π (rather than 0 to π), the potential for water has two equivalent minima and the ground-state wave function has equal amplitude in both of the minima. If the hydrogen atom that is to be treated classically is placed on the positive x-axis, the wave packet will have two peaks, one that is localized at $\theta = 104.5°$ and another at 255.5°. In our studies of the quantum dynamics of the photodissociation of water in the planar representation, we find that the two contributions to the wave function do not overlap. When an argon atom is introduced, this symmetry is broken, and the hydrogen atom will tend to localize in the quadrant where the argon atom is located. This asymmetry will lead to nonphysical effects in the dynamics and product state distributions. To avoid this problem, when we evaluate the quantum/classical dynamics of the Ar atom, we require that the wave function remain symmetric with respect to the replacement of X and X_{Ar} by $-X$ and $-X_{Ar}$.

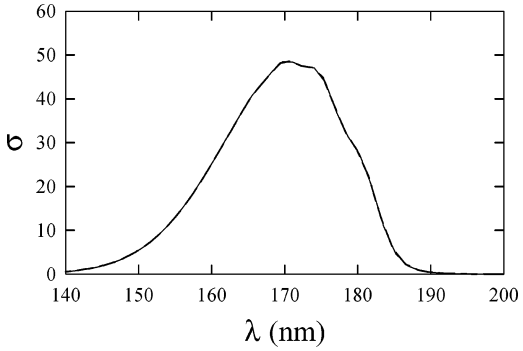

Figure 2. Comparison of the cross sections for the photodissociation of water from ground vibrational state obtained from quantum simulations for the ($J = 0$), solid line, and planar dynamics, dashed line.

III. Results and Discussion

A. Test of the Planar Coordinate Representation. To assess the reliability of the planar coordinate representation for the present study, we performed three-dimensional quantum wave packet simulations of the photodissociation of H_2O from its ground vibrational state in both the planar and Jacobi coordinate representations. The cross sections for photodissociation of H_2O that are obtained from these simulations are shown in Figure 2. By comparing the results of the two simulations, we find that the total cross sections, calculated in the two coordinate representations, are in excellent agreement. The reason for this can be understood fairly easily. The excited state potential energy surface for water is purely repulsive along the dissociation coordinate. As such, the dissociation is direct and prompt. Further, the stretch−bend couplings on this surface are relatively small. Consequently, the shape of the curves in Figure 2 is most sensitive to the projection of the initial wave function onto the H + OH distance coordinate, R. The radial dependence of the Hamiltonians in the two representations differs by a term that is proportional to $1/R^2$, and this term goes to zero as the molecule dissociates. We have also compared the partial cross sections of different final vibrational states of OH and similar agreement is found.

The partial cross sections for $v_{OH} = 0$ and different rotational states of OH are plotted in Figure 3 when $\lambda = 166$ and 193 nm. We choose to focus on these wavelengths as they are of experimental interest and have been used in previous theoretical studies on the photodissociation of water.[49,50] Further, 166 nm is close the maximum of the cross section, while 193 nm corresponds to the low-energy tail of the total cross section. In the case of the planar simulations, the relevant angular

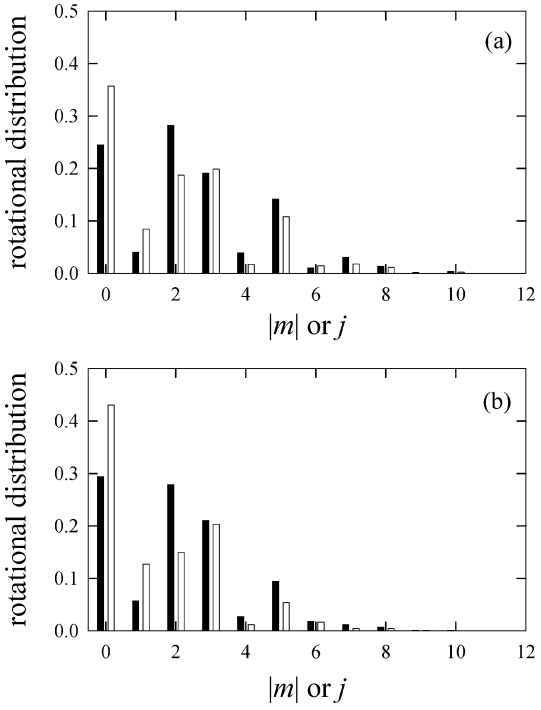

Figure 3. Comparison of the partial cross sections for the photodissociation of water from ground vibrational state obtained from quantum simulations for the ($J = 0$), white bars, and planar dynamics, black bars, when $\lambda =$ (a) 166 nm and (b) 193 nm.

momentum quantum number is m and provides the projection onto the axis that is perpendicular to the H_2O plane. Unlike the usual angular momentum quantum number j (that corresponds to the total angular momentum in the Jacobi coordinate representation), m can be either positive or negative. In the plots in Figure 3, the distributions have been normalized to give a total probability of one.

In both coordinate representations, the OH rotational distributions are structured, and the wavelength dependence of rotational distributions is similar for the two representations. Closer scrutiny of the distributions shows that they are not identical. These similarities and differences can be explained by the fact that we are using different representations of the bending motion. In coordinate space, the probability distributions are identical in the two coordinate representations. In contrast, when we project the ground-state wave function for water onto angular momentum eigenstates, we will obtain slightly different values for the overlap integral when we use Legendre polynomials (that are used in the Jacobi representation) or particle on ring wave functions (that are used in the planar representation). If we compare these distributions to those plotted in Figure 3, we find that this difference in the angular basis accounts for most of the differences between the distributions plotted with black and white bars. This should not be surprising. It has long been recognized that the angular distributions of the OH products from the photodissociation of water reflect the bending vibrations in the initially prepared state. As such, the change in the basis onto which these states are projected accounts for the differences in the final rotational distributions.[51] As in our analysis of the $Ar-H_2O$ dynamics we are primarily interested in changes in the dynamics and product state distributions compared to those obtained for bare water, and we are confident that the planar representation of the photodissociation dynamics will be captured by the most important physics of this system.

B. Photodissociation Dynamics of $Ar-H_2O$. When water is initially in its ground vibrational state, there is equal probability for either of the OH bonds to break. By treating the motions in r and θ quantum mechanically and the motions in **R** and **P** classically, we break the symmetry and impose the bias that the classical OH bond will be the one that is broken. As such, the total cross section, plotted in Figure 4, is twice the cross section that is evaluated in a manner described in the previous section.[52] When we introduce an argon atom, there are two possible choices for its location. The argon atom can be located near to the OH bond that is broken (designated Ar−H−OH), or it can be located near to the OH bond of water that is not broken (Ar−HO−H). The dynamics of these two cases will be different, and, as we choose which bond will be broken in our simulations, these two cases represent the results of two separate sets of quantum/classical simulations.

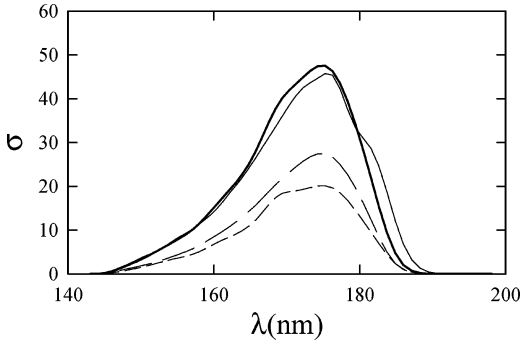

Figure 4. Comparison of the total cross sections for the photodissociation of H_2O (thin line) and $Ar-H_2O$ (thick line). The two contributions to the cross section for $Ar-H_2O$ are plotted with long dashed and short dashed lines for the Ar−HO−H and Ar−H−OH cases, respectively.

The total cross sections for the photodissociation of H_2O and $Ar-H_2O$ that have been obtained from the two-configuration quantum/classical method are plotted in Figure 4. Here, the total cross section for the photodissociation of $Ar-H_2O$ is obtained by adding the cross sections that are obtained from simulations of the Ar−H−OH and Ar−HO−H dynamics.

There are several notable features. First, the total cross section, obtained when we start in the Ar−HO−H configuration, is larger than when the argon atom is placed near to the hydrogen atom that is dissociating. When the argon atom is closer to the OH bond that is broken, it inhibits the dissociation process by introducing a repulsive contribution to the $\tilde{A}$ state potential along the OH distance coordinate.

In addition, when the partial cross sections for the two cases are added together, we find that the presence of the argon atom leads to a blue-shift in the photodissociation cross section, particularly at the longest wavelengths. This effect is not seen at shorter wavelengths. These trends reflect the solvation of the water by the argon atom. On the $\tilde{X}$ state, the $Ar-H_2O$ complex is stabilized by 143 cm^{-1}.[35] Taken alone, this will lead to a shift in the cross section of less than 0.5 nm at the wavelengths plotted here. The $\tilde{A}$ state potential will also be perturbed by the presence of the Ar atom. When the OH bond length is near its equilibrium value or slightly shorter, the Ar−OH interaction will be slightly attractive. Therefore at short wavelengths, the cross section is relatively insensitive to the presence of the argon atom. In contrast, when the length of the OH bond is increased, the Ar−OH potential becomes repulsive due to the short-range Ar−H interaction. As the OH bond is stretched the energy difference between the $\tilde{X}$ and $\tilde{A}$ states will increase, and these factors will lead to the observed blue shift at lower energies.

We have also investigated changes to the rotational distributions brought about by the presence of the argon atom. While

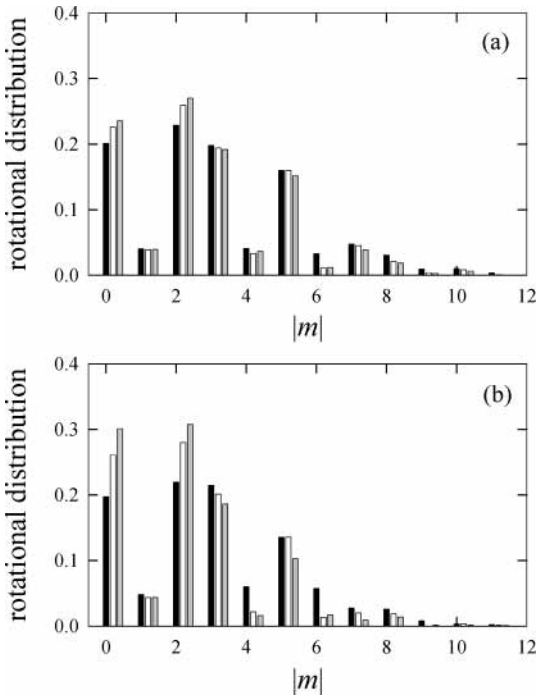

Figure 5. Partial cross sections for the photodissociation of H_2O (white bars) and Ar−H_2O for the Ar−HO−H (black bars) and Ar−H−OH (grey bars) cases when λ = (a) 166 nm and (b) 193 nm.

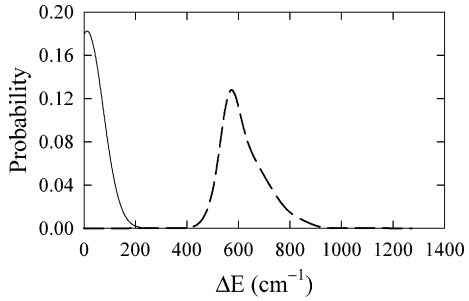

Figure 6. Energy transfer to Ar atom after photodissociation of Ar−H_2O for the Ar−HO−H (solid line) and Ar−H−OH (dashed line) cases.

we have looked at a range of wavelengths, we focus on two, 166 and 193 nm, in the present discussion. The rotational distributions, calculated for these wavelengths, are plotted in Figure 6. As with the total cross sections, we calculate and plot the rotational distributions for the two possible positions of the argon atom separately. When the argon atom is placed closer to the OH bond that remains intact, we observe a slightly warmer OH product distribution. While the effect is seen at both wavelengths, it is more pronounced at 193 nm. When the argon atom is placed in the other position (near the OH bond that is broken), the OH product distribution becomes slightly colder.

These effects can be understood in terms of the energetics of the Ar−OH interaction. When the argon atom is closer to the OH bond that is broken, some of the H + OH recoil energy will be transferred to the argon atom, leaving less energy available for internal motions of the remaining OH. In contrast, when the OH bond that is near the argon atom is left intact, the H−OH interaction will push the OH toward the argon atom, leading to a modest amount of rotational excitation of the OH that remains. This latter case is analogous to the one that has been studied in previous experimental and classical studies of the photodissocation of H_2O and Ar−H_2O.[4,5,27,28]

While differences in the initial states make direct comparisons to these studies difficult. In those studies, the free OH bond is initially excited to its second overtone, and then this bond is selectively broken by a 248 nm photon. In that case, the average rotational energy of the remaining OH is increased from 96(7) to 134(7) cm^{-1}, while the quasiclassical results show a much more modest increase in the rotational energy when the argon atom is introduced.[28] This situation corresponds closely to our calculations of the photodissociaiton of the Ar−HO−H configuration at 193 nm. From the calculations of the rotational energy obtained from the quantum/classical simulations of water ($J = 0$), we obtain an average rotational energy of 125 cm^{-1}. When we constrain the dynamics to a plane, this value increases to 179 cm^{-1}, while the introduction of the argon atom further increases the energy to 244 cm^{-1}. This ratio is roughly equal to that obtained from the experiment. This agreement should be taken with caution since the planar approximation is likely to lead to an increase in the energy transfer among the atoms and therefore increase the amount of rotational excitation of the OH. Despite this, the observed increase in the calculated angular momentum transfer to the OH fragment, compared that obtained by classical dynamics, is encouraging given the differences between experiment and calculation for this quantity and the fact that the same excited state potential surface has been used for the two studies. There are clearly quantum mechanical effects in the product OH rotational distributions, specifically the alteration in the lower and higher probability with m seen in Figures 3 and 5 as well as in the constraints on the values of the rotational energy of the OH fragment imposed by quantization, and it is not surprising that these differences will also lead to differences between the quantum and classical rotational energies of the OH fragments from dissociation of water and the argon−water complex.

A second possible source of the cooling of the OH products when the free OH bond is broken can be seen in the kinetic energy distributions for the argon atom, plotted in Figure 6. When the OH bond that is farther away from the argon atom is broken, only a modest amount of energy is transferred to the argon atom, while when the other OH bond is broken, on average, 600 cm^{-1} is transferred to the argon atom. The distribution of the argon atom kinetic energy mimics the hydrogen atom kinetic energy in this case, scaled by roughly their mass ratio. As this is more than the change in the rotational energies of the products, it provides a second contribution to the changes in the rotational energies of the OH when the free and bonded OH bonds are broken.

IV. Conclusions

In this paper, we presented the results of a multiple-configuration quantum/classical study of the photodissociation dynamics of Ar−H_2O and H_2O. We began the investigation with a study of the accuracy of a planar coordinate representation of the dynamics. We found that the total cross sections are nearly identical in these two coordinate representations. While the rotational distributions display differences, these can be understood in terms of projections of the initially prepared state of water onto the appropriate bend basis functions.

These results gave us confidence for using the planar coordinate Hamiltonian for a comparative study of the photodissociation dynamics of H_2O and Ar−H_2O. We found that the presence of the argon atom causes a blue shift in the low energy part of the total cross section. The rotational distributions for the OH that remain after photodissociation show small perturbations compared to the uncomplexed case, and while the differences are small they are consistent with the changes observed by Nesbitt and co-workers who report an increase in

the population of states with higher angular momentum for the photodissociatin of $Ar-H_2O$, compared to bare H_2O.[27,28] In contrast to the present studies, the experiments focused on the photodissociation of vibrationally excited water molecules. Quantum/classical studies of the photodissociation dynamics and cross sections of vibrationally excited states of water are currently underway.

Acknowledgment. The authors would like to thank Professor J. M. Bowman for providing us with the $Ar-H_2O$ potentials used in this study. The National Science Foundation (CHE-0200968) and the Dreyfus Foundation awards program are gratefully acknowledged for partial support of this work. This paper is dedicated to the memory of Gert D. Billing.

References and Notes

(1) Gerber, R. B.; McCoy, A. B.; Garcia-Vela, A. *Annu. Rev. Phys. Chem.* **1994**, *45*, 275.
(2) Amatatsu, Y.; Mororkuma. *Chem. Phys. Lett.* **1995**, *245*, 469.
(3) Schroder, T.; Schinke, R.; Mandziuk, M.; Bačić, Z. *J. Chem. Phys.* **1994**, *100*, 7239.
(4) Christoffel, K. M.; Bowman, J. M. *J. Chem. Phys.* **1996**, *104*, 8348.
(5) Christoffel, K. M.; Bowman, J. M. *Adv. Mol. Vib. Collision Dyn.* **1998**, *3*, 61.
(6) McCoy, A. B. *J. Chem. Phys.* **1995**, *103*, 986.
(7) McCoy, A. B.; Wang, L.; Chen, F. *Faraday Discuss.* **2001**, *118*, 281.
(8) Wang, L.; McCoy, A. B. *J. Chem. Phys.* **2003**, *119*, 1996.
(9) Garcia-Vela, A.; Gerber, R. B.; Buck, U. *J. Phys. Chem.* **1994**, *98*, 3518.
(10) Auer, B. M.; McCoy, A. B. *J. Phys. Chem. A* **2003**, *107*, 4.
(11) Sanford, T.; Andrews, D.; Rathborne, J.; Taylor, M.; Muntean, F.; Thompson, M.; McCoy, A. B.; Parson, R.; Linberger, W. C. *Faraday Discuss.* **2004**, *127*.
(12) Alimi, R.; Gerber, R. B.; Hammerich, A. D.; Kosloff, R.; Ratner, M. A. *J. Chem. Phys.* **1990**, *93*, 6484.
(13) Gerber, R. B.; Alimi, R. *Isr. J. Chem.* **1991**, *31*, 383.
(14) Gerber, R. B.; Buch, V.; Ratner, M. A. *J. Chem. Phys.* **1982**, *77*, 3022.
(15) Wang, L.; McCoy, A. B. *Phys. Chem. Chem. Phys.* **1999**, *1*, 1227.
(16) Billing, G. D. *Chem. Phys. Lett.* **1983**, *100*, 535.
(17) Billing, G. D.; Jolicard, G. *J. Phys. Chem.* **1984**, *88*, 1820.
(18) Billing, G. D. *J. Chem. Phys.* **2001**, *114*, 6641.
(19) Balakrishnan, N.; Billing, G. D. *Chem. Phys. Lett.* **1995**, *233*, 145.
(20) Wang, L.; Kalyanaraman, C.; McCoy, A. B. *J. Chem. Phys.* **1999**, *110*, 11221.
(21) Makri, N.; Miller, W. H. *J. Chem. Phys.* **1987**, *87*, 5781.
(22) Meyer, H. D.; Manthe, U.; Cederbaum, L. S. *Chem. Phys. Lett.* **1990**, *165*, 73.
(23) Wang, L.; Clary, D. C. *Chem. Phys. Lett.* **1996**, *262*, 284.
(24) Wang, L. *J. Chem. Phys.* **1998**, *108*, 7538.
(25) Wang, L.; Meurer, W. J.; McCoy, A. B. *J. Chem. Phys.* **2000**, *113*, 10605.
(26) Chen, F.; McCoy, A. B. *J. Phys. Chem.* **2003**, *107*, 7220.
(27) Plusquellic, D. F.; Votava, O.; Nesbitt, D. J. *J. Chem. Phys.* **1994**, *101*, 6356.
(28) Votava, O.; Plusquellic, D. F.; Myers, T. L.; Nesbitt, D. J. *J. Chem. Phys.* **2000**, *112*, 7449.
(29) Engel, V.; Schinke, R.; Staemmler, V. *J. Chem. Phys.* **1988**, *88*, 129.
(30) Engel, V.; Schinke, R. *J. Chem. Phys.* **1988**, *88*, 6831.
(31) Henriksen, N. E.; Zhang, J.; Imre, D. G. *J. Chem. Phys.* **1988**, *89*, 5607.
(32) Henriksen, N. E.; Engel, V.; Schinke, R. *J. Chem. Phys.* **1987**, *86*, 6862.
(33) Guo, H.; Murrell, J. N. *Mol. Phys.* **1988**, *65*, 821.
(34) Partridge, H.; Schwenke, D. W. *J. Chem. Phys.* **1997**, *106*, 4618.
(35) Cohen, R. C.; Saykally, R. J. *J. Chem. Phys.* **1993**, *98*, 6007.
(36) Slavíček, P.; Nachtigallová, D.; Jungwirth, P. *Chem. Phys. Lett.* **1999**, *300*, 561.
(37) Jungwirth, P. Private communication.
(38) Kosloff, R. *J. Phys. Chem.* **1988**, *92*, 2087.
(39) Tal-Ezer, H.; Kosloff, R. *J. Chem. Phys.* **1984**, *81*, 3967.
(40) Kosloff, D.; Kosloff, R. *J. Comput. Phys.* **1983**, *52*, 35.
(41) Colbert, D. T.; Sibert, E. L., III. *J. Chem. Phys.* **1989**, *91*, 350.
(42) Brown, R. C.; Heller, E. J. *J. Chem. Phys.* **1981**, *75*, 186.
(43) Wigner, E. *Phys. Rev.* **1932**, *40*, 749.
(44) Hammerich, A. D.; Kosloff, R.; Ratner, M. A. *Chem. Phys. Lett.* **1990**, *171*, 97.
(45) Gray, S. K.; Wozny, C. E. *J. Chem. Phys.* **1989**, *91*, 7671.
(46) Kulander, K. C.; Heller, E. J. *J. Chem. Phys.* **1978**, *69*, 2439.
(47) Neuhauser, D.; Baer, M.; Judson, R. S.; Kouri, D. J. *J. Comput. Phys. Commun.* **1991**, *63*, 460.
(48) Feit, M. D.; Fleck, J. A.; Steger, A. J. *J. Comput. Phys.* **1982**, *47*, 412.
(49) Von Dirke, M.; Schinke, R. *Chem. Phys. Lett.* **1992**, *196*, 51.
(50) Haeusler, D.; Andresen, P.; Schinke, R. *J. Chem. Phys.* **1987**, *87*, 3949.
(51) Schinke, R.; Vander Wal, R. L.; Scott, J. L.; Crim, F. F. *J. Chem. Phys.* **1991**, *94*, 283.
(52) Wang, D.; Zhu, W.; Zhang, J. Z. H.; Kouri, D. J. *J. Chem. Phys.* **1997**, *107*, 751.